JOURNAL OF COMPUTATIONAL PHYSICS 66, 294–323 (1986)

Numerical Studies of Toroidal Resistive Magnetohydrodynamic Instabilities

R. G. STORER

School of Physical Sciences,
The Flinders University of South Australia,
Bedford Park, South Australia 5042

Received April 20, 1983; revised June 19, 1985

DEDICATED TO THE MEMORY OF RAYMOND C. GRIMM

A time-stepping code has been constructed to study the dominant resistive magnetohydrodynamic (MHD) instability of an axisymmetric toroidal plasma. The model used is based on the linearized, incompressible MHD equations with constant density and includes the toroidal ideal model if the resistivity is taken to be zero. The equations are solved fully implicitly using a coordinate system for which one set of coordinate surfaces coincides with a set of surfaces of constant poloidal flux. This is crucial for the accurate representation of modes for which the perturbed quantities vary rapidly near surfaces with rational values of the safety factor. The code is checked by comparison with an exactly soluble model, cylindrical resistive MHD codes and a toroidal ideal MHD code (ERATO). Results are presented showing the effect of resistivity on the unstable internal modes near $nq_0 = 1$ for an INTOR-like numerically generated equilibrium.

1. INTRODUCTION

Over the past decade there have been considerable advances made in the numerical study of ideal magnetohydrodynamic (MHD) instability for toroidal plasmas [1–5]. The most successful of these approaches [1, 2] have used the energy principle and coordinate systems based on the MHD equilibrium flux surfaces. In addition, codes have been developed for a circular plasma column including the effect of resistivity [6–10]. It is not possible to use the energy principle in the same way for this case (see, however, [11, 12]), but the modes can be determined by looking for the parameter values for which the boundary conditions are satisfied, or, for the fastest growing mode, by calculating the long time behaviour of the system. Calculations of the resistive case have also been applied to straight systems including nonlinear effects [13, 14] and coupling between various helicities [15]. These latter codes have used simplified models directed towards the study of disruptive instabilities.

For the development of our knowledge of the behaviour of toroidal plasmas it is important to complement these codes by the study of the case of a fully toroidal plasma. Progress has been made for this problem using Cartesian or polar coor-

0021-9991/86 $3.00

dinates [16, 17] and also flux coordinates [18, 19]. A program to numerically implement the boundary layer matching method [20–23] in toroidal geometry has been successful for zero-pressure systems [24]. In this paper we describe a code, RESAU, which has been developed to integrate the linear equations of resistive MHD for toroidal plasma dynamics using a coordinate system based on the flux surfaces of an axisymmetric pressure balance equilibrium. The code is valid for a wide range of values of the plasma β, aspect ratios and shapes without internal seperatices for both ideal and resistive plasmas. Care has to be taken for very low aspect ratio plasmas (e.g., less than 3) because of the distortion of the flux coordinate system. This is a problem also with other codes which use a similar Jacobian [1, 2]. The introduction of even a small amount of resistivity changes the structure of the equations from hyperbolic to parabolic with the effect of the dissapative terms being felt mainly in what may be termed "internal boundary layers" in the vicinity of rational q-surfaces [20–22]. The code is fully implicit; the parabolic nature of the equations makes implicit methods desirable from the point of view of both computer time and numerical stability. Since the boundary layers occur in the region of particular constant flux surfaces and since they become quite narrow for large values of the magnetic Reynolds number, the choice of a flux-based coordinate system becomes quite important to maintain numerical accuracy. In addition, boundary conditions at the magnetic axis and at the plasma surface can be quite accurately represented using flux coordinates.

The code we have developed can be used to find the fastest growing unstable mode since this mode quickly dominates the solution as time progresses [4, 5, 7, 8]. The problem is not self-adjoint and so the fastest growing mode could be overstable (i.e., have a complex eigenfrequency) in contrast to the ideal case where self-adjointness guarantees that the squares of the characteristic frequencies are real. The cases we discuss in this paper, however, have real growth rates.

2. Basic Equations

We use the following linearized MHD equations (S.I. units):

$$\rho \frac{\partial}{\partial \tau} \delta \mathbf{v} = -\nabla \delta p + \frac{1}{\mu_0} (\nabla \times \mathbf{B}) \times \delta \mathbf{B} + \frac{1}{\mu_0} (\nabla \times \delta \mathbf{B}) \times \mathbf{B}, \tag{2.1}$$

$$\frac{\partial \delta B}{\partial \tau} = \nabla \times (\delta \mathbf{v} \times \mathbf{B}) - \nabla \times \left[\frac{\eta}{\mu_0} \nabla \times \delta \mathbf{B} \right] \tag{2.2}$$

with

$$\nabla \cdot \delta \mathbf{B} = 0. \tag{2.3}$$

Here $\delta \mathbf{B}$, $\delta \mathbf{v}$, and δp are the perturbations on the equilibrium magnetic field ($\mathbf{B}$), velocity and pressure. These equations have been written in the simplest form which

includes the effects of a possibly nonuniform resistivity η. We will neglect the effects of the other transport coefficients and regard the density ρ as a constant.

Since the study of toroidal effects on the stability of resistive plasmas is a complex one, we make the additional assumption that the plasma is incompressible. Studies of ideal MHD instabilities show that compressibility is not a crucial factor in determining the fastest growing mode particularly near the marginal point but affects primarily the structure of the stable part of the spectrum. If the major effect of resistivity is in the neighborhood of surfaces with rational values of the safety factor, q, then it is to be expected that much useful information can be obtained from the study of an incompressible plasma [6–10]. Incompressibility implies

$$\nabla \cdot \delta \mathbf{v} = 0, \tag{2.4}$$

so that the Eqs. (2.1)–(2.3) can be closed (i.e., δp eliminated) by taking the curl of the Eq. (2.1) to obtain

$$\rho \frac{\partial}{\partial \tau} (\nabla \times \delta \mathbf{v}) = \frac{1}{\mu_0} \nabla \times (\mathbf{B} \cdot \nabla \delta \mathbf{B} + \delta \mathbf{B} \cdot \nabla \mathbf{B}). \tag{2.5}$$

To set up the equations in dimensionless form we introduce a characteristic magnetic field amplitude, B_0, which is chosen to be the toroidal magnetic field in the vicinity of the magnetic axis, and a characteristic length, r_p, which is chosen to be half the width of the plasma. With these choices there are two characteristic time scales, defined by the resistive diffusion time

$$\tau_R = r_p^2 \mu_0 / \eta_0 \tag{2.6}$$

(η_0 is the resistivity at the magnetic axis) and the toroidal Alfvén transit time

$$\tau_A = r_P (\mu_0 \rho)^{1/2} / B_0. \tag{2.7}$$

The magnetic Reynolds number, S, is the ratio of these, i.e.,

$$S = \tau_R / \tau_A. \tag{2.8}$$

We shall choose the basic time scale for the problem to be τ_A and put

$$\mathbf{v} = \tau_A \, \delta \mathbf{v} / r_p, \tag{2.9}$$

$$\mathbf{b} = \delta \mathbf{B} / B_0, \tag{2.10}$$

and

$$t = \tau / \tau_A. \tag{2.11}$$

Using these variables, the basic equations are

$$\frac{\partial}{\partial t}(\nabla \times \mathbf{v}) = \nabla \times (\tilde{\mathbf{B}} \cdot \nabla \mathbf{b} + \mathbf{b} \cdot \nabla \tilde{\mathbf{B}}), \tag{2.12}$$

$$\frac{\partial b}{\partial t} = \nabla \times (\mathbf{v} \times \tilde{\mathbf{B}}) - \nabla \times (\tilde{\eta} \nabla \times \mathbf{b}), \tag{2.13}$$

$$\nabla \cdot \mathbf{b} = 0, \tag{2.14}$$

and

$$\nabla \cdot \mathbf{v} = 0, \tag{2.15}$$

where $\mathbf{B} = \tilde{\mathbf{B}}/B_0$ is the normalized equilibrium magnetic field and $\tilde{\eta} = \eta \times (\rho/\mu_0)^{1/2}/r_p B_0$ (note that $1/S = \tilde{\eta}$ at the magnetic axis).

The approach used by Dibiase and Killeen [7] was to take an additional curl of the Eq. (2.12) and to eliminate the toroidal components of both **b** and **v** by using Eqs. (2.14) and (2.15). This was the original approach used by us [18], with the contravariant components of **v** and **b** being used as the basic variables. However, it suffers from several drawbacks. First, in toroidal geometry, using flux coordinates, third order derivatives with respect to the flux coordinate are introduced; second, it was found that for a particular model (the Shafranov constant current model [25]) nonunique solutions are obtained even in the cylindrical limit. This causes serious problems near the magnetic axis where accurate determination of the poloidal components of **b** and **v** are required to suppress any singular behaviour of the toroidal components. Finally, high order derivatives of the equilibrium fields are introduced by the extra differentiation.

The following alternative approach was adopted. The conditions, Eqs. (2.14) and (2.15), were satisfied exactly by introducing vector potentials for both **b** and **v**, i.e., we introduce **a** and **u** so that

$$\mathbf{b} = \nabla \times \mathbf{a} \tag{2.16}$$

and

$$\mathbf{v} = \nabla \times \mathbf{u}. \tag{2.17}$$

This does not define **a** and **u** uniquely; however, we can resolve this by choosing the toroidal component of **u** to be zero and requiring **a** to be solution of the equation

$$\frac{\partial \mathbf{a}}{\partial t} = (\nabla \times \mathbf{u}) \times \mathbf{B} + \nabla(\mathbf{B} \cdot \mathbf{u}) - \eta(\nabla \times \nabla \times \mathbf{a}), \tag{2.18}$$

i.e., we absorb the gradient of the arbitrary function, introduced when Eq. (2.13) is integrated, into **a** itself. (Note the ~ has been dropped at this point.) The additional

term involving the gradient of the scalar function $\mathbf{B}\cdot\mathbf{u}$ simplifies the component form of the right-hand side of Eq. (2.18) and in particular, for an ideal eigenmode, forces $a_\phi \propto u_\phi$. This equation along with

$$\frac{\partial}{\partial t}(\nabla\times\nabla\times\mathbf{u}) = \nabla\times(\mathbf{B}\cdot\nabla(\nabla\times\mathbf{a}) + (\nabla\times\mathbf{a})\cdot\nabla\mathbf{B}) \tag{2.19}$$

(which is Eq. (2.12) written in terms of $\mathbf{a}$ and $\mathbf{u}$) then constitute the basic equations which are satisfied by the poloidal components of $\mathbf{u}$ and the three components of $\mathbf{a}$. The compressible case could be treated by introducing an additional term in Eq. (2.17) in the form of the gradient of a scalar potential and taking the gradient of Eq. (2.1) and the continuity equation as the additional two equations needed to determine the scalar potential and the perturbed pressure. One significant advantage of the set of equations we use is that the resistivity can be taken to be non-uniform without introducing derivatives of the resistivity. For example, a vacuum region outside of the plasma could be simulated by choosing the resistivity to be large in that region [16].

3. Coordinate System

The choice of the toroidal coordinate system is important. For most tokamaks the magnetic Reynolds number, S, is large. Analytic treatments [20–23] have shown that under this condition the predominant effect of resistivity is in a narrow region in the vicinity of rational q surfaces. Thus, as we have emphasized, to have any hope of treating instabilities for even moderate values of S, a coordinate system must be chosen for which the coordinate surfaces coincide with the flux surfaces of the equilibrium plasma. This problem was faced by the designers of some codes for ideal toroidal MHD stability studies [1–3] and we use a modification of the coordinate system used in the Princeton PEST code. Starting with a numerical equilibrium solver, this enables the mapping section [1] of that code to be used with minor changes to provide starting data for our code.

In the Princeton scheme the magnetic field is expressed in the form

$$\mathbf{B} = B_0[f\nabla\phi\times\nabla\psi + Rg\nabla\phi], \tag{3.1}$$

where ϕ is the toroidal angle; ψ labels the magnetic surfaces and is chosen so that $\psi = 0$ at the magnetic axis and $\psi = 1$ at the plasma surface. The function $f(\psi)$ is related to the poloidal flux function $\Psi(\psi)$ by

$$f = \frac{1}{2\pi B_0}\frac{\partial\Psi}{\partial\psi}. \tag{3.2}$$

If X, ϕ, Z are the usual cylindrical coordinates, with $\hat{\mathbf{Z}}$ defining the symmetry axis

and the magnetic axis lying in the $Z=0$ plane, the toroidal component of the magnetic field is related to $g(\psi)$ via

$$B_{\text{tor}} = B_0 Rg/X, \tag{3.3}$$

so that it is convenient to choose R to be the distance of the magnetic axis from the axis of symmetry and then $g=1$ at the magnetic axis.

We choose ϕ and ψ as two of the coordinates of the toroidal coordinate system. The third coordinate θ is chosen to simplify the operation $\mathbf{B}\cdot\nabla$. The Jacobian, J, is given by

$$J = (\nabla\phi \times \nabla\psi \cdot \nabla\theta)^{-1} \tag{3.4}$$

and the safety factor, q, by

$$q(\psi) = \frac{d\Phi}{d\psi} = \frac{Rg}{2\pi f}\oint J/X^2\, d\theta, \tag{3.5}$$

where Φ is the toroidal flux function and the integral over θ is taken over a constant ψ and ϕ line. With these definitions the operator $\mathbf{B}\cdot\nabla$ is

$$\begin{aligned}\mathbf{B}\cdot\nabla &= \mathbf{B}\cdot\nabla\theta\frac{\partial}{\partial\theta} + \mathbf{B}\cdot\nabla\phi\frac{\partial}{\partial\phi} \\ &= \frac{B_0 f}{J}\left[\frac{\partial}{\partial\theta} + \frac{2\pi J/X^2}{\int J/X^2\, d\theta}\, q\frac{\partial}{\partial\phi}\right],\end{aligned} \tag{3.6}$$

where we have used the condition $0 \leqslant \theta < 2\pi$.

Note that we have used the toroidal Alfven transit time (τ_A), i.e., with respect to the toroidal magnetic field at the magnetic axis, as the basic time scale. Comparison with cylindrical models [25] and other ideal MHD results [1–3] is often more conveniently made in terms of the poloidal Alfvén transit time (i.e., with respect to a weighted average of the poloidal magnetic field at the plasma surface) which is taken to be $\tau_A r_p/q_s R$, where q_s is the safety factor at the plasma surface.

The choice

$$J = X^2/\alpha(\psi), \tag{3.7}$$

where $\alpha(\psi)$ is an arbitrary function of ψ leads to

$$JB\cdot\nabla = B_0 f\left(\frac{\partial}{\partial\theta} + q\frac{\partial}{\partial\phi}\right), \tag{3.8}$$

i.e., the field lines are straight in this new coordinate system. It is expected that this will lead to a greater accuracy in the representation of this operator numerically when one works with Fourier transforms with respect to θ and ϕ [1].

The function $\alpha(\psi)$ could be chosen to concentrate the grid points in regions

where the solutions vary significantly, e.g., in the region of rational q values. This refinement may become necessary for the treatment of larger values of S. Two cases are of interest: first, $\alpha =$ constant will give the coordinate system used in the initial PEST code [1]. This has the disadvantage for our purposes that in the large aspect ratio, cylindrical limit where the Jacobian is approximately constant

$$\psi \propto r^2, \tag{3.9}$$

where r is the radial distance from the magnetic axis. This makes our formulation of the boundary conditions awkward (with factors of $\psi^{1/2}$ appearing [1]) and leads to a large spacing in the ψ grid near the magnetic axis. It has proved more satisfactory to use

$$\alpha \propto \frac{1}{\psi}, \tag{3.10}$$

for which, in the above limit,

$$\psi \propto r, \tag{3.11}$$

which gives a more accurate representation in a finite difference formulation near the magnetic axis. This coordinate system is close to that used in the ERATO code [2].

The decomposition of the basic vectors $\mathbf{u}$ and $\mathbf{a}$ has been made in terms of their covariant components [26]. Thus we express

$$\mathbf{u} = u_\psi \nabla\psi + u_\theta \nabla\theta + u_\phi \nabla\phi \tag{3.12}$$

and

$$\mathbf{a} = a_\psi \nabla\psi + a_\theta \nabla\theta + a_\phi \nabla\phi. \tag{3.13}$$

Since the coordinate system we use is nonorthogonal, the components of Eqs. (2.18) and (2.19) are not simple and need to be calculated by exploiting various vector identities and the use of such expressions as

$$J(\nabla \times \mathbf{a})^\psi = \frac{\partial a_\phi}{\partial\theta} - \frac{\partial a_\theta}{\partial\phi} \tag{3.14}$$

(with cyclic permutations of ψ, θ, ϕ),

$$J\nabla \cdot \mathbf{a} = \frac{\partial}{\partial\psi}(Ja^\psi) + \frac{\partial}{\partial\theta}(Ja^\theta) + \frac{\partial}{\partial\phi}(Ja^\phi) \tag{3.15}$$

and

$$a_i = \sum_i g_{ik} a^k, \tag{3.16}$$

where the metric tensor components

$$g^{\psi\psi} = |\nabla\psi|^2,$$
$$g^{\psi\theta} = g^{\theta\psi} = \nabla\psi \cdot \nabla\theta,$$
$$g^{\theta\theta} = |\nabla\theta|^2, \tag{3.17}$$

and

$$g^{\phi\phi} = 1/X^2,$$

are obtained as output from a mapping code as functions of ψ and θ; along with f, g, and q as functions of ψ. The covariant components of the metric tensor ($g_{\psi\psi}$, etc.) are obtained from the inverse of the contravariant tensor (Eq. (3.17)). Future modifications of the code envisage the use of an equilibrium solver which uses flux coordinates [26, 27] to obtain this metric information directly and quickly.

4. Reduction of the Basic Equations

Fourier analysis of the components of the vectors **u** and **a** can be used to express their dependence on the variables θ and ϕ and to simplify the expressions involved. Because of the axisymmetry of the equilibrium, the toroidal modes decouple and, in what follows, we treat each toroidal mode independently. Thus we take

$$u_\psi(\psi, \theta) = \sum_l i u_{\psi l}(\psi) \exp[i(l\theta - n\phi)], \tag{4.1}$$

$$u_\theta(\psi, \theta) = \sum_l u_{\theta l}(\psi) \exp[i(l\theta - n\phi)], \tag{4.2}$$

$$u_\phi(\psi, \theta) = \sum_l u_{\phi l}(\psi) \exp[i(l\theta - n\phi)], \tag{4.3}$$

$$a_\psi(\psi, \theta) = \sum_l a_{\psi l}(\psi) \exp[i(l\theta - n\phi)], \tag{4.4}$$

$$a_\theta(\psi, \theta) = \sum_l i a_{\theta l}(\psi) \exp[i(k\theta - n\theta)], \tag{4.5}$$

and

$$a_\psi(\psi, \theta) = \sum_l i a_{\phi l}(\psi) \exp[i(l\theta - n\phi)]. \tag{4.6}$$

Note that we have followed the notation of Ref. [1] in that l is the poloidal mode number, in contrast to the notation m, which is often in cylindrical geometry. The parameter n is the toroidal mode number.

The factor i is included explicitly in the analysis of u_ψ, a_θ, and a_ϕ because, in the

common case, of symmetry about the $Z=0$ plane, the real and imaginary terms decouple and we can treat the Fourier components, as defined, as being real quantities.

Because of the factor J appearing on the left-hand side of Eqs. (3.14) and (3.15) it is convenient to multiply the Eqs. (2.18) and (2.19) by this factor before taking their Fourier transform. After this Fourier analysis the three contravariant components of Eq. (2.19) can be written in the form

$$\begin{aligned}\frac{\partial}{\partial t}\sum_l\sum_\beta\Bigg[& R_{1\alpha\beta}(l', l, \psi)\, u_{\beta l} + R_{2\alpha\beta}(l', l, \psi)\frac{\partial u_{\beta l}}{\partial \psi} \\ & + R_{3\alpha\beta}(l', l, \psi)\frac{\partial^2 u_{\beta l}}{\partial \psi^2}\Bigg] \\ = \sum_l\sum_\beta\Bigg[& P_{1\alpha\beta}(l', l, \psi)\, a_{\beta l} + P_{2\alpha\beta}(l', l, \psi)\frac{\partial a_{\beta l}}{\partial \psi} \\ & + P_{3\alpha\beta}(l', l, \psi)\frac{\partial a^2_{\beta l}}{\partial \psi^2}\Bigg],\end{aligned} \tag{4.7}$$

where the subscripts α and β take on values which correspond to the ψ, θ, and ϕ components, respectively, and the indices l and l' label the appropriate Fourier coefficients. Equation (2.18) yields

$$\begin{aligned}\frac{\partial}{\partial t}\sum_l [J_{l'-l}(\psi)\, a_{\alpha l}] & \\ = \sum_l\sum_\beta [W_{\alpha\beta}(l', l, \psi)\, u_{\beta l}] & \\ - \eta\sum_l\sum_\beta\Bigg[& Q_{1\alpha\beta}(l', l, \psi) a_{\beta l} + Q_{2\alpha\beta}(l', l, \psi)\frac{\partial a_{\beta l}}{\partial \psi} \\ & + Q_{3\alpha\beta}(l', l, \psi)\frac{\partial^2 a_{\beta l}}{\partial \psi^2}\Bigg],\end{aligned} \tag{4.8}$$

where $J_l(\psi)$ refers to the lth Fourier coefficient in the expansion of the Jacobian.

There are a large number of terms involved in the calculation of most of the coefficients and these are listed in Appendix A. In the course of this calculation it is necessary to carry out numerical differentiation of the metric tensor elements, etc., with respect to θ and ψ. The θ derivatives are evaluated using fast Fourier transform techniques and the ψ derivatives by using Lagrange interpolation, the order of which can be chosen arbitrarily so that one can determine the dependence of the final result on the order used in this aspect of the calculation. Typically a value of 4 has been used.

Because of the freedom we have in the choice of the velocity stream function $\mathbf{u}$, we can choose the toroidal component of $\mathbf{u}$ to be zero, which means that we need

only determine five sets of Fourier components, viz. $u_{\psi l}$, $u_{\theta l}$, $a_{\psi l}$, $a_{\theta l}$, $a_{\phi l}$ ($l=0, \pm 1, \pm 2,...$). We therefore only need to retain five sets of equations from Eqs. (4.7) and (4.8). For convenience we choose only the ψ- and θ-components from Eq. (4.7), the ϕ-component equations being redundant in this case.

5. Finite Difference Form

The Eqs. (4.7) and (4.8) can be approximated by introducing N equally spaced grid points for the ψ range (0, 1) and making, e.g., the substitution

$$\left.\frac{\partial u_{\psi l}}{\partial \psi}\right|_j = (u_{\psi l, j+1} - u_{\psi l, j-1})/2\nabla\psi, \tag{5.1}$$

$$\left.\frac{\partial^2 u_{\psi l}}{\partial \psi^2}\right|_j = (u_{\psi l, j+1} - 2u_{\psi l, j} + u_{\psi l, j-1})/(\nabla\psi)^2, \tag{5.2}$$

where $\nabla\psi = 1/(N-1)$ and $\psi_j = (j-1)\nabla\psi$. Nonequally spaced points could be accommodated but with a lower order of accuracy. For the interior points this will enable the equations to be cast in the following form

$$\frac{\partial}{\partial t}(Ru) = (Pu), \tag{5.3}$$

where R and P are matrices of block tridiagonal form and u represents the solution vector (incorporating both $u_{\alpha l, j}$ and $a_{\alpha l, j}$ over the whole range of values of α, l, and j. It will be useful to introduce "zone-packing" so that there will be more grid points in the vicinity of the rational surfaces, where the eigenfunctions may vary rapidly. This modification is being introduced for future versions of the code; however, the numerical process remains essentially the same. Using a fully implicit time differencing procedure we can write

$$Ru^{k+1} - Ru^k = (1-\varepsilon)\,\Delta t\, Pu^{k+1} + \varepsilon\,\Delta t\, Pu^k, \tag{5.4}$$

where the implicitness parameter ε is usually taken to be $\frac{1}{2}$ and the superscript k refers to the value of the solution at the kth time-step. This set of equations can be cast into the form

$$-A_j u_{j+1}^{k+1} + B_j u_j^{k+1} - C_j u_{j-1}^{k+1} = d_j^k, \qquad j=2,..., N-1, \tag{5.5}$$

where A_j, B_j, and C_j are square matrices whose order depends on the number of Fourier modes retained. If $l_{\min} < l < l_{\max}$ and $L = l_{\max} - l_{\min} + 1$, then these matrices are of order $5L \times 5L$. The vector d_j^k is determined entirely from the solution at the kth time step, via $(R + g\,\Delta t P)\,u^k$. In the next section it will be shown that the boundary conditions can also be cast into this form but with $C_1 = 0$ and $A_N = 0$.

Those equations need to be solved repeatedly and an efficient scheme has been

set up, based on the standard procedure (see Dibiase [7] or Potter [28]). The technique has been optimized so that the set of $5L \times 5L$ matrices have to be inverted only once. These inverses and other required quantities are stored on disk and only a series of matrix-vector multiplications (of order $5L$) are required at each step of the iteration procedure (see Appendix B). This saves both space and time and each time step takes a time of order NL^2. (On the Flinders University PRIME 750, the actual time per step is approximately $0.01NL^2$ sec.)

6. Boundary Conditions

The form of the boundary condition at the magnetic axis will depend on the behaviour of J near $\psi = 0$. If we choose $J \sim \psi$ (see Eqs. (3.7) and (3.10)) then the appropriate boundary conditions are

$$u_{\psi l} \sim a_{\psi l} \sim \psi^{||l|-1|}, \tag{6.1}$$

$$u_{\theta l} \sim a_{\theta l} \sim \psi^{||l|-1|+1}, \tag{6.2}$$

$$a_{\phi l} \sim \psi^{|l|}. \tag{6.3}$$

These relations can be obtained most readily by studying the cylindrical or large-aspect ratio case and are equivalent to the boundary conditions used for toroidal MHD codes [1, 2]. Thus the simple way of expressing the boundary conditions, at the magnetic axis for each step, is, e.g.,

$$\begin{aligned} u_{\theta l,1} &= a_{\theta l,1} = 0, \\ u_{\psi l,1} &= a_{\psi l,1} = 0 \qquad (l \neq 1), \\ -u_{\psi l,2} + u_{\psi l,1} &= 0 \qquad (l = 1), \end{aligned} \tag{6.4}$$

and

$$-a_{\psi l,2} + a_{\psi l,1} = 0 \qquad (l = 1).$$

These equations can then be expressed compactly in the same form as Eq. (5.5) viz.

$$-A_1 u_2^{k+1} + B_1 u_1^{k+1} = d_1^k, \tag{6.5}$$

where d_1^k is taken to be zero, B_1 is the unit matrix and A_1 has zero components except for the components which correspond to the ψ-component equations for $l = 0$.

The boundary conditions at the conducting wall are subject to some debate [7–10] and it would be useful to study the effect of different boundary conditions, which will depend to some extent on the assumptions made about the plasma con-

ditions near the wall. Numerically, it is useful to choose boundary conditions which are consistent with the basic equations (2.18) and (2.19), i.e., that do not lead to large derivatives in the immediate vicinity of the boundary. In practice, therefore, we have chosen the set used by Dibiase and Killeen [7, 8] which express the conditions which hold when there is a vacuum between the plasma and the wall, in the limit as the vacuum layer thickness approaches zero. Thus we take the normal components of the perturbed magnetic field, velocity, current and vorticity to be zero, i.e.,

$$v^{\psi} = 0, \tag{6.6}$$

$$b^{\psi} = 0, \tag{6.7}$$

$$(\nabla \times \mathbf{v})^{\psi} = 0, \tag{6.8}$$

$$(\nabla \times \mathbf{b})^{\psi} = 0. \tag{6.9}$$

In addition these conditions are appropriate for a direct comparison to be made with the ideal MHD code ERATO [2] when the wall is taken next to the plasma. The contravariant ψ components of $(\nabla \times \mathbf{b})$ or $(\nabla \times \nabla \times \mathbf{a})$ and $(\nabla \times \mathbf{v})$ or $(\nabla \times \nabla \times \mathbf{u})$ involve only the first derivatives of the components of $\mathbf{a}$ and $\mathbf{u}$ (see Appendix A) and so these conditions lead to well-defined mixed boundary conditions.

A fifth condition is required to close the equations. When η is equal to zero we note that the ϕ-component of Eq. (2.18) involves only u_{ϕ} on the right-hand side (see Eqs. (4.8) and (A.2)). Since we choose the gauge with $u_{\phi} = 0$, it is therefore consistent to fix

$$a_{\phi} = 0 \tag{6.10}$$

on the wall when we look for a normal mode. When η is not equal to zero it is not self-consistent to take $a_{\phi} = 0$. However, we note that the contravariant ψ component of the complete right-hand side of Eq. (2.18) involves only the first derivatives, with respect to ψ, of the components of $\mathbf{a}$ and $\mathbf{u}$. Hence this equation can be set up in finite difference form at the wall with the left-handed first derivatives to close the equations.

Applying these conditions at the wall we are led to four sets of conditions which can be expressed in the form (for each value of l')

$$\sum_{l} \sum_{\beta} \left[X_{1\alpha\beta}(l', l)\, u_{\beta l} + X_{2\alpha\beta}(l', l) \frac{\partial u_{\beta l}}{\partial \psi} \right]\Bigg|_{\psi = 1} = 0, \qquad \alpha = \psi, \theta, \tag{6.11}$$

$$\sum_{l} \sum_{\beta} \left[Y_{1\alpha\beta}(l', l)\, a_{\beta l} + Y_{2\alpha\beta}(l', l) \frac{\partial a_{\beta l}}{\partial \psi} \right]\Bigg|_{\psi = 1} = 0, \qquad \alpha = \psi, \theta, \phi; \tag{6.12}$$

where $\beta = (\psi, \theta, \phi)$ and the coefficients $X_{1\alpha\beta}$, $X_{1\alpha\beta}$, $Y_{1\alpha\beta}$, and $Y_{2\alpha\beta}$ are given in Appendix A. The fifth conditions follows from the appropriate combinations of the

equations (4.8). Expressing the ψ-derivative as a left-handed finite difference form, these equations can be cast in the form

$$B_N u_N^{k+1} - C_N u_{N-1}^{k+1} = d_N^k, \tag{6.13}$$

where d_N^k is taken to be zero at each time-step. This equation, along with Eqs. (6.5) and (5.5), completes the setting up of the implicit iteration scheme in a block tridiagonal form.

7. Iteration Procedure

There is a great deal of freedom in the choice of the initial function u^0. If we are using the iteration to project out the fastest growing mode, u^0 needs only to be not orthogonal to this mode. If the resistivity is chosen to have a very large value outside a certain flux surface, this outside region will correspond to a fixed vacuum region surrounding the plasma. In such a case it would be appropriate to choose the initial u^0 such that there were no currents in this region by, for example, choosing the initial vector potential to be zero in this region. If no information is known about the structure of the sought-for mode, a simple quadratic form multiplied by ψ^l or ψ^{l+1} (see Eqs. (6.1), (6.2)) is chosen for the components of $\mathbf{u}$ and $\mathbf{a}$. Alternatively, if a series of parameter changes are being made, it saves considerable time if u^0 for the new parameter value is chosen to be the iterated solution for the previous run.

After a sufficient number of iterations, k_s, for a purely unstable case, the fastest growing mode will dominate and

$$u^{k+1} = \lambda u^k, \tag{7.1}$$

where λ is independent of k for $k > k_s$. Provided that Δt is sufficiently small, λ has the form

$$\lambda = \exp(\gamma\, \Delta t), \tag{7.2}$$

and we could therefore find the growth rate λ from

$$\gamma \approx \log \lambda / \Delta t \approx \log \left[\frac{\|u^{k+1}\|}{\|u^k\|} \right] \Big/ \Delta t, \tag{7.3}$$

where $\|u\|$ represents some reasonable norm of the vector u, e.g., the square root of the sum of the squares of the components. In practice we can calculate γ for each component of u separately and require that these agree to some predetermined accuracy. When resistivity is included, the symmetry properties, which guarantee that γ^2 is real for the ideal case, do not exist. Thus, circumstances can arise for which the characteristic modes have both an exponentially growing and an

oscillatory character. Effectively this implies that the characteristic time dependency is described by a complex γ. Such cases require a special treatment.

A procedure which is accurate for larger values of Δt, and hence may require a smaller number of iterations, can be obtained by utilizing the structure of the basic iteration equation, Eq. (5.4), for the case $\varepsilon = \frac{1}{2}$. In fact the iteration scheme Eq. (5.4) can be regarded as equivalent to a scheme which projects out the eigenvector corresponding to the largest eigenvalue of the matrix $(R + \frac{1}{2}P\,\Delta t)/(R - \frac{1}{2}P\,\Delta t)$. If γ is the eigenvalue corresponding to $Pu = \gamma Ru$, then

$$\lambda = (1 + \tfrac{1}{2}\gamma\,\Delta t)/(1 - \tfrac{1}{2}\gamma\,\Delta t), \tag{7.4}$$

This is true for almost any Δt ($\neq 2/\gamma$), however, it is clearly advantageous to choose Δt close to $2/\gamma$. This is equivalent to the inverse iteration procedure [28] and can considerably reduce the number of iterations. One does have to take care, however, that the Δt is not chosen in a way which projects out the higher (less unstable) eigenmodes. At the present time this can only be done by trial and error as the non-hermiticity of the matrices does not permit (as is done for the ideal MHD codes [1, 2]) a direct check on the number of modes with a growth rate larger than a nominated amount. The procedure therefore is to iterate Eq. (5.4) until one mode dominates and to estimate the growth rate γ from

$$\gamma = \frac{2(\lambda - 1)}{\Delta t(\lambda + 1)}. \tag{7.5}$$

If the system is overstable, i.e., the growth rate is complex, we follow a procedure of Wilkinson [29] in which the mutual inner products of three successive iterates are used to set up the coefficients of a quadratic equation whose roots give an estimate of γ. In practice this procedure is used normally since there is no a priori reason to believe that the growth rate will be real, although this is usually the case. Ryu and Grimm [6] (see also [24]) give some counterexamples for a cylindrical model.

8. Results

We present results from a variety of situations, to show the validity of RESAU and to explore toroidal effects on resistive instabilities. It is expected to publish later more complete parameter studies. First, a comparison with the analytic results from an exactly soluble resistive MHD model [30] is presented. In this model the plasma equilibrium is cylindrical and has a constant axial current and a constant axial magnetic field. With constant resistivity this is an extension of the model of Shafranov [24] and the growth rates γ (in units of the poloidal Alfvén time) of the characteristic modes are given by

$$\gamma(\gamma - (\zeta^2 + \kappa^2)/S) = \left(\frac{\kappa}{nq}\right)^2 \left[-(l - nq)^2 \pm \frac{2(l - nq)\kappa}{\sqrt{\zeta^2 + \kappa^2}} \right], \tag{8.1}$$

where ζ is a parameter which, to satisfy conducting wall boundary conditions, must be a solution to the transcendental equation

$$\kappa\zeta J_l'(\zeta) \pm (\zeta^2 + \kappa^2)\, l J_l(\zeta) = 0, \tag{8.2}$$

where, in both equations, the sign is chosen consistently. Here $\kappa = nr_P/R$ can be regarded as the dimensionless wave number in the axial direction. The cylindrical limit is simulated in this case by taking the following metric tensor components (r_p = plasma radius)

$$\begin{aligned} g^{\psi\psi} &= 1/r_p^2, \\ g^{\psi\theta} &= g^{\theta\psi} = 0, \\ g^{\theta\theta} &= 1/r_p^2\psi^2, \\ g^{\phi\phi} &= 1/R^2 \end{aligned} \tag{8.3}$$

with the Jacobian

$$J = r_p^2 R\psi \qquad (0 < \psi < 1) \tag{8.4}$$

and, for this model, g and q are constant and $f(\psi) = gr_p^2\psi/q$.

The ideal MHD result corresponds to the case $\eta \to 0$. If ζ is small, the plasma is unstable (γ real and positive) for the same ranges of values of the parameters (κ, l, q) that apply for the ideal case. Otherwise the plasma perturbations are either purely damped (γ real and negative) or damped and oscillating (γ complex with a negative real part). Unfortunately, this model, which has no shear (i.e., q is constant), does not display any of the complexity which is seen in other models (Refs. [7, 21]). In fact the limit $\eta \to 0$ is a uniform one, so that the model does not exhibit tearing mode behaviour, which is characterized by almost singular eigen-

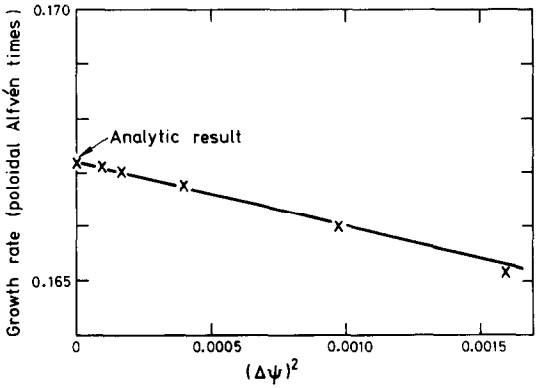

FIG. 1. Showing a comparison between the analytic result and the numerical result extrapolated to $\Delta\psi = 0$. The approximately linear part of the curve corresponds to values of $N \geqslant 50$.

functions near rational q-surfaces. However, it does serve to point out that tearing mode behaviour does not necessarily occur when q has a rational value. We shall present cases with shear, in toroidal geometry, which exhibit simple resistively modified ideal MHD instabilities even in the vicinity of values of q which are equal to the ratio of small integers. The finite difference procedures used in Section 5 for variations in the ψ-direction are second-order accurate so that the numerical result should differ from the analytic result by an amount of order $(\Delta\psi)^2$. This result is illustrated in Fig. 1, showing that a realistic comparison with the analytic result should only be made after extrapolation. The parameters used for this comparison were $q = 1.4$, $n = 1$, $l = 1$, $\eta = 0.01$ and $\kappa = 1.4$.

This model is also used to explore the scaling with respect to Δt. In particular it is of interest to compare the result for the growth rate γ obtained by using the approximation of Eq. (7.3), which relies on the smallness of Δt and in practice is only accurate for $\gamma\,\Delta t \ll 1$, and the estimate given by Eq. (7.5), which will give an accurate estimate of the eigenvalue of $Pu = \gamma Ru$ for almost any values of Δt. The choice of an appropriate value of Δt therefore will depend on the magnitude of the growth rate of the mode of interest. This is obviously easier if one has an estimate of the growth rate for the mode, so it is often worthwhile to carry out a series of runs with a small number of grid points and poloidal modes. This is more difficult near the marginal points; however, often a series of growth rates are required for varying parameter values and extrapolation from known growth rates can give sufficiently accurate estimates of the growth rate to enable good choices to be made for Δt.

In Table I the growth rate obtained using Eq. (7.3) is given, among with the growth rate obtained using Eq. (7.5), for the constant current model case con-

TABLE I

Study of Effect of Change of Δt on Growth Rate γ

Δt	λ	$\log \lambda/\Delta t$	γ	n_t
2.5	1.586	0.1844	0.1812	39
5.0	2.657	0.1955	0.1812	20
10.0	20.29	0.3010	0.1812	8
15.0	−6.569	—	0.1812	16
20.0	3.770	0.06635	0.05808	80
25.0	6.300	0.07362	0.05808	13
50.0	−5.425	—	0.05808	15
100.0	6.971	0.01942	0.01498	12

Note. A study, for the constant current model with $q = 1.1$, $n = 1$, $l = 1$, $\eta = 0.01$, $\kappa = 1.4$, and $N = 71$, of the effect of the change of Δt on the growth rate, γ, calculated using Eq. (7.5), compared with $\log \lambda/\Delta t$ (which is valid only for small values of Δt and many time-steps n_t). Note that as Δt is increased, the less unstable modes are projected out. The exact values, from Eq. (8.1), for the growth rates of the 3 most unstable modes are 0.1808, 0.05706, and 0.01920, respectively; for direct comparison with these values one would have to extrapolate in N (see Fig. 1).

sidered above with $N = 71$. The figures under n_t represent the number of iterations required to achieve a predetermined accuracy in the eigenfunction (less then 0.01% average change in an iteration in this case). Note that an accurate growth rate can be found using Eq. (7.3) only for quite small values of Δt, and hence for a correspondingly large number of iterations. It will be noted that a wide range of values of Δt can be chosen if Eq. (7.5) is used to estimate the growth rate, but clearly the choice of $\Delta t \approx 2/\gamma$ will minimize the number of iterations required. However, one does have to take care because a wrong choice of Δt may project out a mode other than the one of interest. For example if γ_1 and γ_2 are the growth rates of two distinct modes then if

$$|(1 + \tfrac{1}{2}\gamma_2 \Delta t)/(1 - \tfrac{1}{2}\gamma_2 \Delta t)| > |(1 + \tfrac{1}{2}\gamma_1 \Delta t)/(1 - \tfrac{1}{2}\gamma_1 \Delta t)| \tag{8.5}$$

then the second mode will be obtained in preference to the first. This is illustrated in Table I for $\Delta t \geqslant 20.0$.

The toroidal extension of this constant current model is the Solov'ev model [31], for which the equilibrium current is strictly inversely proportional to the distance X from the central axis. Detailed studies have been made for this model for the ideal MHD case [32, 33, 34] and thus a comparison with these results should give a check of those parts of the code which correspond to the ideal equations (i.e., all except the second term on the right-hand side of (4.8)). Unfortunately this is not completely straightforward because these published results included the effect of compressibility and, in its present form, our code treats only an incompressible plasma. However, if a sufficiently large value of the specific heat ratio is chosen then the ERATO code can be used to give reliable results for incompressible toroidal plasmas. In practice it was found that an increase in the specific heat ratio above 10,000 leads to minimal changes in the calculated growth rate. The results of this code have been compared with those obtained from ERATO, with this modification, for the Solov'ev equilibria with aspect ratio 3 and toroidal mode number $n = 2$. For this equilibrium, the ratio $q_s/q_0 = 1.74$, where q_s and q_0 are the safety factor values on the surface and at the magnetic axis [32, 33, 34].

The two codes are quite different in structure and so for each case the results have to be extrapolated to give comparable results. In the case of ERATO [2] the extrapolation is to the limits N_ψ and $N_\chi \to \infty$ and in the case of RESAU we need to extrapolate in N (the number of surfaces in the ψ direction) in the manner indicated in Fig. 1 and choose a sufficiently large value of L (the number of poloidal modes). Due to limitations of computer space and time the number of poloidal Fourier modes needs to be restricted. It proved useful to centre the poloidal modes which were included around the dominant mode number. This can often be estimated before the calculation, because usually $nq_0 < l_{\text{dominant}} < nq_s$ for a case where q is a monotonically increasing function. This relatively low-aspect-ratio case studied has significant toroidal effects and hence considerable poloidal mode coupling. Table II illustrates the effect of increasing the number of poloidal modes, L, with various

TABLE II

Growth Rate for Low Aspect Ratio Solov'ev Case

l_{max} \ l_{min}	-1	-2	-3	-4
2	0.07586	0.07601	0.07613	0.07618
3	0.08059	0.08075	0.08087	0.08093
4	0.08298	0.08315	0.08328	0.08334
5	0.08403	0.08420	0.08434	0.08440
6	0.08447	0.08464	0.08478	0.08484

Note. The growth rate, as a function of the poloidal modes chosen, for a low aspect ratio Solov'ev case (aspect ratio 3, $n=2$, $N=51$, $q_0=0.5$).

values of l_{min} for the case where $q_0=0.50$. Convergence is not uniform with increasing l_{max}; however, it can be seen that the result for 10 poloidal modes centred on $l=1$ would be unlikely to change by more than 0.5% by including more poloidal modes. The case chosen here is particularly sensitive as it is near a marginal point.

Table III compares the results for the code RESAU with the results from ERATO for a fixed boundary for various Solov'ev equilibria. These runs are facilitated by using the scaling factor which enables one to transform one equilibrium into another (giving various values for q_0) without repeating the mapping procedure [35, 2]. In the case of ERATO the result is obtained by an extrapolation using $(N_\psi, N_\chi)=(40, 20)$ and $(60, 30)$ and assuming quadratic convergence [2]. The results for RESAU are shown for various values of (l_{min}, l_{max}). This comparison gives some confidence that the parts of the code which are included in the ideal MHD equations, including all the toroidal coupling terms, are correct. It is worthwhile noting here that the resistive terms which arise from the term $\eta(\nabla\times\nabla\times\mathbf{a})$ on the right-hand side of Eq. (2.18) are essentially a repetition of

TABLE III

Growth Rate Squared γ^2 for Solov'ev Model

q_0	$L=7$ $l_{min}=-2$ $l_{max}=4$	$L=8$ -2 5	$L=9$ -3 5	ERATO
0.5	0.0579	0.0595	0.0597	0.0608
0.45	0.1025	0.1042	0.1055	0.1055
0.40	0.1647	0.1670	0.1675	0.1680
0.35	0.2289	0.2328	0.2328	0.2347

Note. With aspect ratio 3 and toroidal mode number 2, obtained from RESAU with various numbers of poloidal modes (L); compared with the results from ERATO. Both sets of results are obtained by extrapolation assuming quadratic convergence.

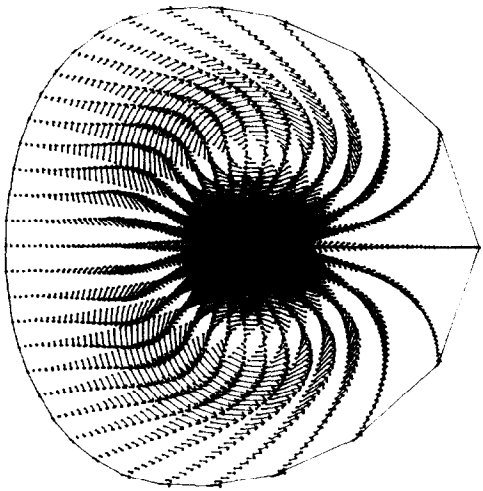

FIG. 2. Poloidal projection of the velocity vectors of the most unstable mode for a Solov'ev model—ideal case ($\eta = 0.0$, $q_0 = 0.45$, $n = 2$, aspect ratio 3). The distortion of the smooth boundary shape is an artifact of the plotting routine.

the coding which is used to construct the left-hand side of Eq. (2.19), viz. $(\nabla \times \nabla \times \mathbf{u})$, which is part of the ideal MHD equation set. To give some idea of the timing it may be noted that for the parameters $N = 71$, $L = 7$, it takes 14 min on the Flinders University PRIME 750 to set up the matrix coefficients, 7 min to construct the inverse matrix transformation and 30 sec/time-step of the iteration (with perhaps 10 iterations for a well chosen value of Δt). These times scale as NL^2.

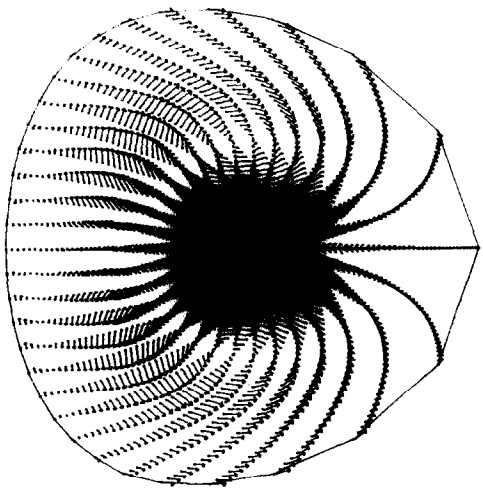

FIG. 3. Poloidal projection of the velocity vectors of the most unstable mode for a Solov'ev model—resistive case ($\eta = 0.01$, $q_0 = 0.45$, $n = 2$, aspect ratio 3).

For the Solov'ev model the growth rates of the unstable resistive modes approach uniformly the ideal growth rates as η is reduced, as was found for the circular constant current case. This applies even when there are singular surfaces ($l = n - q$) in the plasma. For example, for the above case with $q_0 = 0.45$ and $n = 2$, nq ranges from 0.9 to 1.56. For moderately large values of the restivity ($\eta = 0.01$) the unstable modes differ from the ideal modes, but only slightly. Examples are shown of the poloidal projection of the velocity vectors for a Solov'ev model; Fig. 2 for the ideal case and Fig. 3 for the resistive case ($\eta = 0.01$). The onset of the greater differences between the resistive result and the ideal result seems to be associated with the presence of a low-order singular surface in the vicinity of the magnetic axis. In this case, this occurs when $q_0 = 0.5$ (i.e., $nq_0 = 1$), where the mode structure is dominated by an $l = 1$ internal mode.

The modes so far discussed correspond to simple resistively modified ideal modes. To study resistive tearing modes we turn to the Bessel function model. This model corresponds to a zero beta, reverse field pinch (RFP) equilibrium. This model has been studied in some detail by Dibiase and Killeen [7, 8]. For this model, in our

functions. Figure 4 shows the poloidal projection of the velocity vectors of the unstable mode for a typical $l = 1$ tearing mode with $\eta = 0.0005$. This case corresponds to the somewhat artificial situation with $r_p = 5.5$, where there is a reversal in the poloidal field. However, at the singular surface, where $l - nq = 0$,

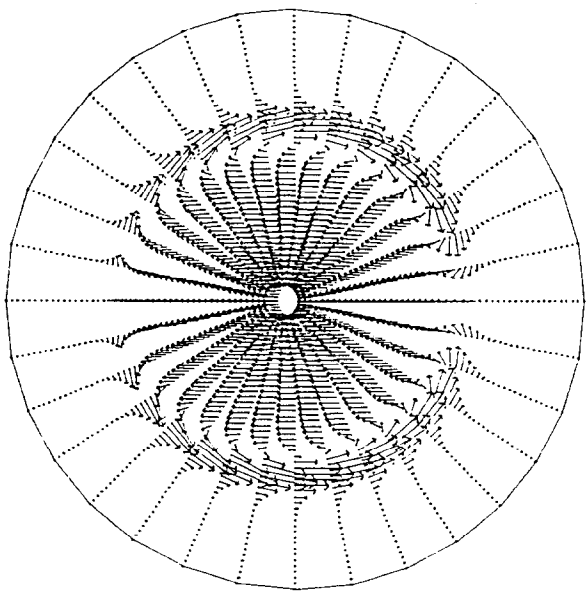

FIG. 4. Poloidal projection of the velocity vectors of the most unstable mode for a Bessel function model—resistive case ($\eta = 5 \times 10^{-4}$, $l = 1$, $r_p = 5.5$, $n/R = -0.2$). Note the "tearing" across the singular surface.

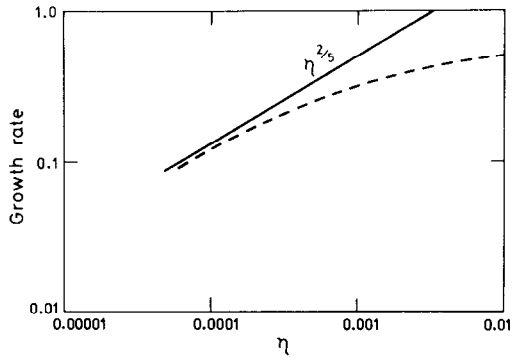

FIG. 5. Growth rate as a function of η. For comparison the asymptotic form $\eta^{2/5}$ is also shown.

"tearing" occurs with an abrupt change in the direction of the velocity vectors. The critical layer width decreases as η is decreased and it is obviously better to have as large number of grid points as possible, particularly in the neighbourhood of the singular surface. It has been found possible to obtain reasonable results for $\eta = 10^{-4}$ after extrapolation from $N = 100$. It is quite possible to use more points than this in a cylindrical calculation, however, in a fully toroidal case storage and computing time availability has imposed a limitation an N of this order. Boundary

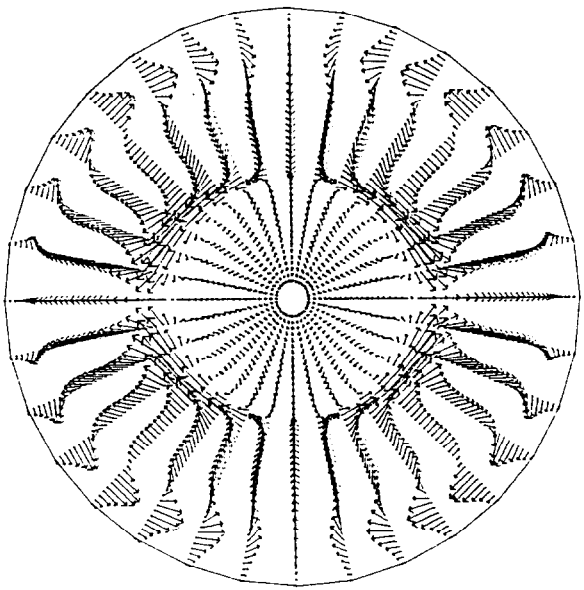

FIG. 6. Poloidal projection of the velocity vectors of the most unstable mode for a Bessel function model—resistive case ($\eta = 5 \times 10^{-3}$, $l = 2$, $r = 7.0$, $n/R = -0.4$). Note the "double tearing" across the two singular surfaces.

layer calculations [20] show that the growth time should scale as $\eta^{2/5}$ for small η. We have found, as have also Dibiase and Killeen [7] and Ryu and Grimm [6] that values of η less than 10^{-4} are required before this asymptotic sealing law is reached. Figure 5 shows a plot of the growth rate as a function of η for this case. One result of interest is the occurrence of "double tearing" modes which can occur in situations where the profile of q produces two singular surfaces. Figure 6 shows the poloidal projection of the velocity vectors at $\phi = 0$ for a double tearing mode corresponding to the case $l = 2$, $r_p = 7.0$, $n_R = -0.4$, $\eta = 5 \times 10^{-3}$ for the Bessel function model.

To illustrate the application of this code to the study of the effect of resistivity on the growth rate of a numerically calculated toroidal equilibrium [36], we present results for an equilibrium which is similar to that used in model studies for INTOR [37]. The equilibrium is obtained by numerical solution (using SOR iteration) of the Grad–Shafranov equation for a plasma with boundary shape given by the parametric equations

$$\begin{aligned} X &= R + a\cos(\theta + t\sin\theta), \\ Z &= Ea\sin\theta \end{aligned} \tag{8.5}$$

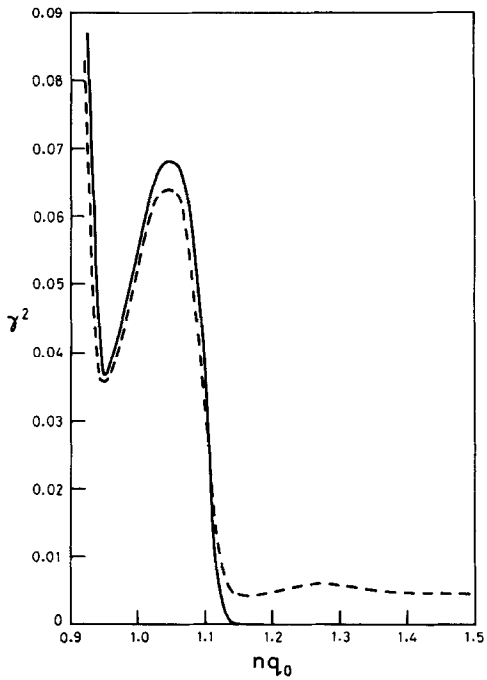

FIG. 7. The growth rate squared for the dominant unstable mode for a series of INTOR-like equilibria. The dashed curve corresponds to the resistive case ($\eta = 10^{-4}$) and the full curve to the ideal case.

with a pressure (p) and toroidal flux function (g) being defined by

$$p(\Psi) = p_0 \Psi^2 + p_1 \Psi^3,$$
$$g^2(\Psi) = t_0 \Psi^2 + t_1 \Psi^3 \tag{8.6}$$

with $\Psi = 0$ on the boundary. For the case studied the major radius $R = 5.2m$, the inverse aspect ratio $a/R = 0.27$, the elongation $E = 1.6$ and the triangularity $t = 0.3$ and the current was chosen so that $\beta \approx 2\%$. Of particular interest is the behaviour near the marginal point, since resistivity may extend the region of instability. Fig. 7

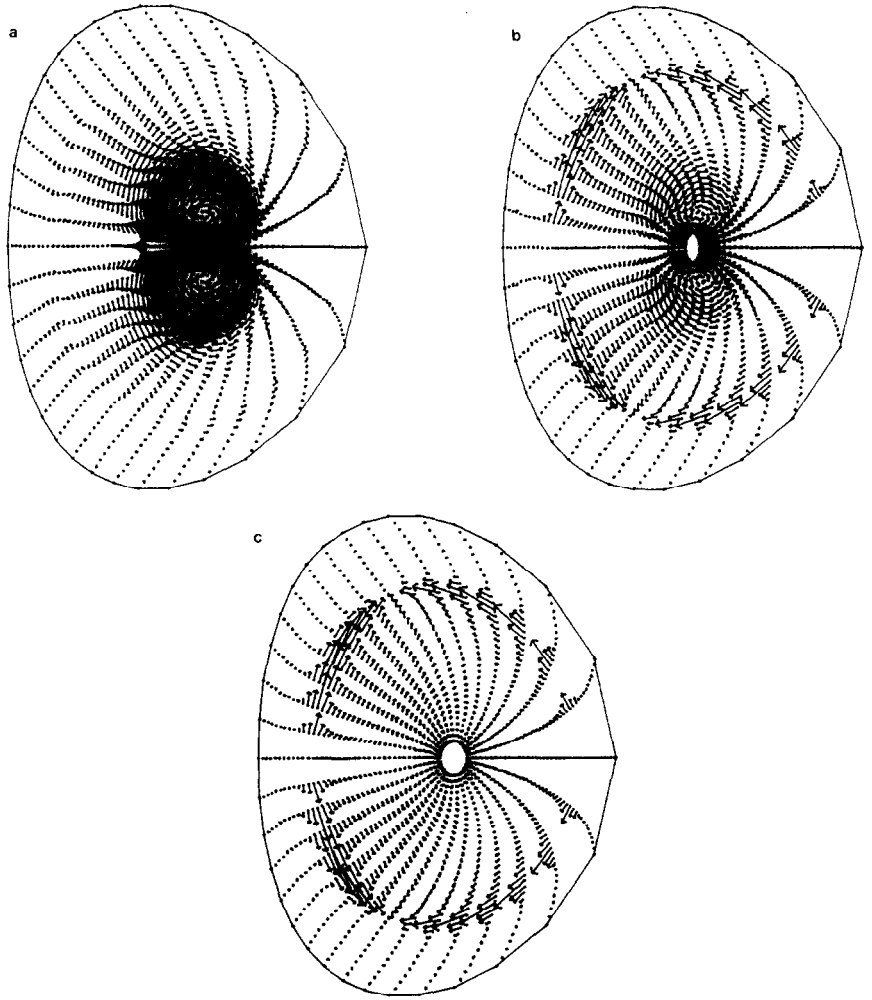

FIG. 8. Poloidal projection of the resistively unstable mode for (a) $nq_0 = 1.092$ (below ideal marginal point), (b) $nq_0 = 1.22$, (c) Poloidal projection of the resistively unstable mode $nq_0 = 1.150$ (above ideal marginal point) for an INTOR-like equilibrium.

shows the growth rate squared (γ^2), as a function of nq_0 (where q_0 is the safety factor at the magnetic axis), for a series we INTOR-like equilibria scaled with the Bateman scaling factor [35]. These results were obtained using $N=71$, $l_{\min}=-1$, $l_{\max}=5$, $n=4$ for both the ideal case ($\eta=0.0$) and the resistive case (with $\eta=10^{-4}$). There is no significant difference in including resistivity for the case where the plasma is ideally unstable; however, in this case the plasma is resistively unstable for the region $nq_0>1.15$, where for practical purposes the plasma is not ideally unstable ($\gamma^2<10^{-4}$). A discussion of the problems of determining the ideal marginal point is given in Ref. [37] and this code faces similar problems for extremely small growth rates. A study of the unstable resistive modes as a function of nq_0 near the ideal marginal point is instructive. Figs. 8a, b, and c show the unstable modes for $nq_0=1.092$, 1.122, and 1.140. For $nq_0<1.092$ the mode is essentially an $l=1$ internal kink (for both the resistive and the ideal case), however, as this mode is ideally stabilized by increasing nq_0, the surface $nq_0=2$ assumes importance and the resistivity induces an unstable layer at this surface, dominated by the $l=2$ poloidal component.

9. Conclusion

This paper has presented only a limited selection of the parameter studies which are possible and it is anticipated that more systematic studies will be forthcoming. Extensions and modifications of RESAU are planned which will treat compressible plasmas and which will search on the complex frequency plane for the complete eigenfrequencies. Such studies have been carried out for cylindrical plasmas by Ryu and Grimm [6] and for toroidal plasmas using a boundary layer approach by Grimm *et al.* and Manickam *et al.* [24].

RESAU has the following important features. The vector potential approach, coupled with the use of flux surfaces the basis for the coordinate system, enables the equation to be set up with, at most, second derivatives and with the possibility of treating large values of the magnetic Reynolds number by increasing the number of coordinate surfaces in the vicinity of a singular surface. Also, derivatives of the resistivity do not appear in the equations. This opens up the possibility of treating a vacuum region outside the plasma as a region of very high resistivity.

APPENDIX A

The coefficients of the Fourier components of $\mathbf{u}$ and $\mathbf{a}$ and their derivatives, which appear in Eqs. (4.7), (4.8), (6.11), and (6.12), can be expressed in terms of the Fourier components of various combinations of the metric tensor elements and the Jacobian, along with the functions $f(\psi)$, $g(\psi)$, $q(\psi)$ and their derivatives. For notational simplicity we have not included below the arguments (l', l, ψ) appropriate for each coefficient and it should be understood that one should choose

the Fourier component (with respect to θ) of order $l'-l$ of the whole right-hand side of each equation. Some simplification has been achieved by using integration by parts to eliminate θ-derivatives where possible and by replacing all ϕ-derivatives of **u** or **a** by the combination $(-in)$, since their ϕ-dependence is always of the form $\exp(-in\phi)$ (see Eqs. (4.1)–(4.6)).

Thus the nonzero terms are (for the left-hand side of Eq. (4.7)):

$$R_{1\psi\psi}=ll'\frac{g_{\phi\phi}}{J}+\frac{n^2 g_{\theta\theta}}{J},\qquad R_{1\psi\theta}=n^2 i\frac{g_{\theta\psi}}{J},\qquad R_{1\psi\phi}=nli\frac{g_{\theta\psi}}{J},$$

$$R_{1\theta\psi}=-n^2 i\frac{g_{\psi\theta}}{J}-l\frac{\partial}{\partial\psi}\left(\frac{g_{\phi\phi}}{J}\right),\qquad R_{1\theta\theta}=n^2\frac{g_{\psi\psi}}{J},\qquad R_{1\theta\phi}=nl\frac{g_{\psi\psi}}{J},$$

$$R_{2\phi\psi}=-l\frac{g_{\phi\phi}}{J},\qquad R_{2\theta\theta}=-\frac{\partial}{\partial\psi}\left(\frac{g_{\phi\phi}}{J}\right),\qquad R_{2\theta\phi}=ni\frac{g_{\psi\theta}}{J},$$

$$R_{3\theta\theta}=-\frac{g_{\phi\phi}}{J},$$

$$R_{1\phi\psi}=n\frac{\partial}{\partial\psi}\left(\frac{g_{\theta\theta}}{J}\right)-nl'i\frac{g_{\psi\theta}}{J},\qquad R_{1\phi\theta}=n\frac{\partial}{\partial\psi}\left(\frac{ig_{\theta\psi}}{J}\right)+nl'\frac{g_{\psi\psi}}{J},$$

$$R_{1\phi\phi}=ll'\frac{g_{\psi\psi}}{J}+il\frac{\partial}{\partial\psi}\left(\frac{g_{\psi\theta}}{J}\right),$$

$$R_{2\phi\psi}=n\frac{g_{\theta\theta}}{J},\qquad R_{2\phi\theta}=n\frac{ig_{\theta\psi}}{J},\qquad R_{2\phi\phi}=-\frac{\partial}{\partial\psi}\left(\frac{g_{\theta\theta}}{J}\right)+(l+l')\frac{ig_{\psi\theta}}{J},$$

$$R_{3\phi\phi}=-\frac{g_{\theta\theta}}{J}. \tag{A.1}$$

For the right-hand side of Eq. (4.8):

$$W_{\psi\psi}=-F=-f(l-nq),\qquad W_{\psi\theta}=\frac{\partial f}{\partial\psi}-\frac{f}{J}\frac{\partial J}{\partial\psi},$$

$$W_{\psi\phi}=\frac{\partial}{\partial\psi}(fq)-\frac{fq}{J}\frac{\partial J}{\partial\psi},$$

$$W_{\theta\theta}=F+i\frac{f}{J}\frac{\partial J}{\partial\theta}=f(l-nq)+i\frac{f}{J}\frac{\partial J}{\partial\theta},\qquad W_{\theta\phi}=i\frac{fq}{J}\frac{\partial J}{\partial\theta}, \tag{A.2}$$

$$W_{\phi\phi}=F=f(l-nq);$$

$$Q_{1\psi\psi}=l\frac{g_{\psi\psi}}{J}i\frac{\partial g_{\phi\phi}}{\partial\theta}+l'lg_{\psi\psi}\frac{g_{\phi\phi}}{J}+n^2\frac{J}{X^2}+lig_{\psi\theta}\frac{\partial}{\partial\psi}\left(\frac{g_{\phi\phi}}{J}\right),$$

$$Q_{2\psi\psi} = lig_{\psi\theta}\frac{g_{\phi\phi}}{J}, \qquad Q_{2\psi\theta} = -lg_{\psi\psi}\frac{g_{\phi\phi}}{J} - ig_{\psi\theta}\frac{\partial}{\partial\psi}\left(\frac{g_{\theta\theta}}{J}\right) + ig_{\phi\phi}\frac{\partial}{\partial\theta}\left(\frac{g_{\psi\psi}}{J}\right),$$

$$Q_{2\psi\phi} = n\frac{J}{X^2},$$

$$Q_{3\psi\theta} = -ig_{\psi\theta}\frac{g_{\phi\phi}}{J},$$

$$Q_{1\theta\psi} = -l'lig_{\psi\theta}\frac{g_{\phi\phi}}{J} + l\frac{\partial g_{\psi\theta}}{\partial\theta}\frac{g_{\phi\phi}}{J} + lg_{\theta\theta}\frac{\partial}{\partial\psi}\left(\frac{g_{\phi\phi}}{J}\right),$$

$$Q_{1\theta\theta} = n^2\frac{J}{X^2}, \qquad Q_{1\theta\phi} = nl\frac{J}{X^2},$$

$$Q_{2\theta\psi} = lg_{\theta\theta}\frac{g_{\phi\phi}}{J}, \qquad Q_{2\theta\theta} = l'ig_{\psi\phi}\frac{g_{\phi\phi}}{J} - \frac{\partial g_{\psi\theta}}{\partial\theta}\frac{g_{\phi\phi}}{J} - g_{\theta\theta}\frac{\partial}{\partial\psi}\left(\frac{g_{\phi\phi}}{J}\right), \tag{A.3}$$

$$Q_{3\theta\theta} = -g_{\theta\theta}\frac{g_{\phi\phi}}{J},$$

$$Q_{1\phi\psi} = -ng_{\phi\phi}\frac{\partial}{\partial\psi}\left(\frac{g_{\theta\theta}}{J}\right) + nl'ig_{\psi\theta}\frac{g_{\phi\phi}}{J} - n\frac{g_{\psi\theta}}{J}\frac{\partial g_{\phi\phi}}{\partial\theta},$$

$$Q_{1\phi\theta} = ng_{\phi\phi}\, i\frac{\partial}{\partial\psi}\left(\frac{g_{\psi\theta}}{J}\right) + nl'g_{\phi\phi}\frac{g_{\psi\psi}}{J} + in\frac{g_{\psi\psi}}{J}\frac{\partial g_{\phi\phi}}{\partial\theta},$$

$$Q_{1\phi\phi} = lig_{\phi\phi}\frac{\partial}{\partial\psi}\left(\frac{g_{\psi\theta}}{J}\right) + l'lg_{\psi\psi}\frac{g_{\phi\phi}}{J} + l\frac{g_{\psi\psi}}{J}\frac{\partial g_{\phi\phi}}{\partial\theta},$$

$$Q_{2\phi\psi} = -ng_{\theta\theta}\frac{g_{\phi\phi}}{J}, \qquad Q_{2\phi\theta} = nig_{\psi\theta}\frac{g_{\phi\phi}}{J},$$

$$Q_{2\phi\phi} = (l'+l)\, ig_{\psi\theta}\frac{g_{\phi\phi}}{J} - g_{\phi\phi}\frac{\partial}{\partial\psi}\left(\frac{g_{\theta\theta}}{J}\right) - \frac{g_{\psi\theta}}{J}\frac{\partial g_{\phi\phi}}{\partial\theta},$$

$$Q_{3\phi\phi} = -g_{\theta\theta}\frac{g_{\phi\phi}}{J}.$$

For the right-hand side of Eq. (4.7):

$$P_{1\psi\psi} = l'lF\frac{g_{\phi\phi}}{J^2} - l'lZ_{\phi\phi} + n^2F\frac{g_{\theta\theta}}{J^2} - n^2Z_{\theta\theta} - nlZ_{\theta\phi},$$

$$P_{1\psi\theta} = -nl'Z_{\phi\psi} - n^2F\frac{ig_{\theta\psi}}{J^2} - n^2Z_{\theta\psi},$$

$$P_{1\psi\phi} = -l'lZ_{\phi\psi} - nlF\frac{ig_{\theta\psi}}{J^2} - nlZ_{\theta\psi},$$

$$
\begin{aligned}
P_{2\psi\theta} &= -l'F\frac{g_{\phi\phi}}{J^2} + l'Z_{\phi\phi} + nZ_{\theta\phi}, \qquad P_{2\psi\phi} = nF\frac{g_{\theta\theta}}{J^2} - nZ_{\theta\theta},\\
P_{1\theta\psi} &= -n^2Fi\frac{g_{\psi\theta}}{J^2} - n^2Z_{\psi\theta} - nlZ_{\psi\phi} - l\frac{\partial}{\partial\psi}\left(F\frac{g_{\phi\phi}}{J^2}\right) + l\frac{\partial}{\partial\psi}(Z_{\phi\phi}),\\
P_{1\theta\theta} &= -n^2F\frac{g_{\psi\psi}}{J^2} - n^2Z_{\psi\psi} + n\frac{\partial}{\partial\psi}(Z_{\phi\psi}),\\
P_{1\theta\phi} &= -nlF\frac{g_{\psi\psi}}{J^2} - nlZ_{\psi\psi} + l\frac{\partial}{\partial\psi}(Z_{\phi\psi}),\\
P_{2\theta\psi} &= -lF\frac{g_{\phi\phi}}{J^2} + lZ_{\phi\phi}, \qquad P_{2\theta\theta} = nZ_{\psi\phi} + \frac{\partial}{\partial\psi}\left(F\frac{g_{\phi\phi}}{J^2}\right) - \frac{\partial}{\partial\psi}(Z_{\phi\phi}) + nZ_{\theta\psi},\\
P_{2\theta\phi} &= -nF\frac{ig_{\psi\theta}}{J^2} - nZ_{\psi\theta} + lZ_{\phi\psi},\\
P_{3\theta\theta} &= F\frac{g_{\phi\phi}}{J^2} - Z_{\phi\phi},\\
P_{1\phi\psi} &= n\frac{\partial}{\partial\psi}\left(F\frac{g_{\theta\theta}}{J^2}\right) - n\frac{\partial}{\partial\psi}(Z_{\theta\theta}) - l\frac{\partial}{\partial\psi}(Z_{\theta\phi}) - nl'F\frac{ig_{\psi\theta}}{J^2} - nl'Z_{\psi\theta} - l'lZ_{\psi\phi}\\
P_{1\phi\theta} &= -n\frac{\partial}{\partial\psi}\left(F\frac{ig_{\psi\theta}}{J^2}\right) + n\frac{\partial}{\partial\psi}(Z_{\theta\psi}) - nl'F\frac{g_{\psi\psi}}{J^2} - nl'Z_{\psi\psi},\\
P_{1\phi\phi} &= -l\frac{\partial}{\partial\psi}\left(\frac{iF}{J^2}g_{\psi\theta} + Z_{\theta\psi}\right) - ll'\left(\frac{F}{J^2}g_{\psi\psi} + Z_{\psi\psi}\right)\\
P_{2\phi\psi} &= nF\frac{g_{\theta\theta}}{J^2} - nZ_{\theta\theta} - lZ_{\theta\phi}, \qquad P_{2\phi\theta} = -nF\frac{ig_{\psi\theta}}{J^2} - nZ_{\theta\psi} + \frac{\partial}{\partial\psi}(Z_{\theta\phi}) + l'Z_{\psi\phi},\\
P_{2\phi\phi} &= -lF\frac{ig_{\psi\theta}}{J^2} + \frac{\partial}{\partial\psi}\left(F\frac{g_{\theta\theta}}{J^2}\right) - lZ_{\theta\psi} - \frac{\partial}{\partial\psi}(Z_{\theta\theta}) - l'F\frac{ig_{\psi\theta}}{J^2} - l'Z_{\psi\theta},\\
P_{3\phi\theta} &= Z_{\theta\phi}, \qquad P_{3\phi\phi} = F\frac{g_{\theta\theta}}{J^2} - Z_{\theta\theta}.
\end{aligned}
\tag{A.4}
$$

In the above expressions we have used the notation $F = f(l - nq)$ and it also proved convenient to use $Z_{\alpha\beta}$ to represent those coefficients of the contravariant components of $J\mathbf{b}$ which do not explicitly involve F, in the expression for the covariant components of $(\tilde{\mathbf{B}}\cdot\nabla\mathbf{b} + \mathbf{b}\cdot\nabla\tilde{\mathbf{B}})$. Explicitly

$$
\begin{aligned}
Z_{\psi\psi} &= \left[\frac{if}{J}\frac{\partial g_{\psi\theta}}{\partial\psi} - \frac{\partial f}{\partial\psi}i\frac{g_{\psi\theta}}{J} - f\frac{\partial}{\partial\psi}\left(i\frac{g_{\psi\theta}}{J}\right) - i\frac{f}{J}\frac{\partial g_{\psi\psi}}{\partial\theta} + f\frac{g_{\psi\psi}}{J^2}i\frac{\partial J}{\partial\theta}\right]\Big/J,\\
Z_{\psi\theta} &= \left[2f\frac{\partial}{\partial\theta}\left(\frac{g_{\psi\theta}}{J}\right) - \frac{f}{J}\frac{\partial g_{\theta\theta}}{\partial\psi}\right]\Big/J,
\end{aligned}
$$

$$
\begin{aligned}
Z_{\psi\phi} &= \left[-\frac{fq}{J} \frac{\partial g_{\phi\phi}}{\partial \psi} \right] \Big/ J, \\
Z_{\theta\psi} &= \left[f \frac{\partial}{\partial \psi} \left(\frac{g_{\theta\theta}}{J} \right) - f \frac{g_{\psi\theta}}{J^2} \frac{\partial J}{\partial \theta} + \frac{\partial f}{\partial \psi} \frac{g_{\theta\theta}}{J} \right] \Big/ J, \\
Z_{\theta\theta} &= \left[fi \frac{\partial}{\partial \theta} \left(\frac{g_{\theta\theta}}{J} \right) - f \frac{g_{\theta\theta}}{J^2} i \frac{\partial J}{\partial \theta} \right] \Big/ J, \qquad Z_{\theta\phi} = \left[-\frac{Rg}{X^2} i \frac{\partial g_{\phi\phi}}{\partial \theta} \right] \Big/ J, \\
Z_{\phi\psi} &= \left[\frac{\partial}{\partial \psi} Rg \right] \Big/ J, \qquad Z_{\phi\phi} = \left[\frac{f}{J} i \frac{\partial g_{\phi\phi}}{\partial \theta} - \frac{f g_{\phi\phi}}{J^2} i \frac{\partial J}{\partial \theta} \right] \Big/ J.
\end{aligned}
\tag{A.5}
$$

The final terms required are those involved in the boundary condition at the wall (Eqs. (6.11) and (6.12). Each of the following terms needs to be evaluated at $\psi = 1$,

$$
\begin{aligned}
&X_{1\psi\theta} = Y_{1\psi\theta} = n, \qquad X_{1\psi\phi} = Y_{1\psi\phi} = l, \\
&X_{1\theta\psi} = Y_{1\theta\psi} = l'l \frac{g_{\phi\phi}}{J} + n^2 \frac{g_{\theta\theta}}{J}, \qquad X_{1\theta\theta} = -Y_{1\theta\theta} = n^2 \frac{ig_{\psi\theta}}{J}, \\
&X_{1\theta\phi} = -Y_{1\theta\phi} = nl \frac{ig_{\psi\theta}}{J}, \\
&X_{2\theta\theta} = -Y_{2\theta\theta} = l' \frac{g_{\phi\phi}}{J}, \qquad X_{2\theta\phi} = -Y_{2\theta\phi} = -n \frac{g_{\theta\theta}}{J}, \\
&Y_{2\phi\phi} = 1.
\end{aligned}
\tag{A.6}
$$

Any term not included in each of the above lists (Eqs. (A.1)–(A.6)) is zero.

The Fourier transforms of the above terms were evaluated using fast Fourier transform techniques, with the number of θ grid points being typically 32, and the results combined to give the set of matrices A, B, and C which make up the total block tridiagonal system.

APPENDIX B

The block tridiagonal system we need to solve repeatedly has the form (see Eqs. (5.5), (6.5), and (6.13)),

$$
-A_j u_{j+1} + B_j u_j - C_j u_{j-1} = d_j, \tag{B.1}
$$

where $j = 1,..., N$ and $C_1 = 0$ and $A_N = 0$. The A's, B's, and C's are matrices of order $M \times M$ with $M = 5L$. The solution can be written as

$$
u_j = E_j u_{j+1} + f_j, \qquad j = 1,..., N-1 \tag{B.2}
$$

and

$$u_N = f_N,$$

where the matrices E_j and the vectors f_j are defined iteratively via

$$E_j = G_j A_j, \qquad j = 2,..., N, \tag{B.3}$$

$$f_j = G_j d_j + G_j C_j f_{j-1}, \qquad j = 2,..., N, \tag{B.4}$$

where

$$G_j = (B_j - C_j E_{j-1})^{-1}, \qquad j = 2,..., N. \tag{B.5}$$

As starting values for this iteration

$$E_1 = B_1^{-1} A_1 \tag{B.6}$$

and

$$f_1 = B_1^{-1} d_1 \tag{B.7}$$

are used.

Having calculated A_j, B_j, and C_j ($j = 1,..., N$), the matrices E_j, G_j, and $G_j C_j$ ($j = 1,..., N$) (with $G_1 = B_1^{-1}$ and $G_1 C_1 \equiv 0$) need only be calculated and stored on disk once, the storage requirement being $3 \times N \times M \times M$. For each time-step we need to use the forward iteration scheme (B.7) and (B.4) to calculate the f's and the backward iteration scheme (B.2) to calculate the u's. Core storage for only 2 of the $M \times M$ matrices is required at each step of the iteration.

ACKNOWLEDGMENTS

The author is grateful to the late Raymond Grimm for significant inspiration, encoragement, and advice and for permission to modify for use modules from the PEST code. This paper is dedicated to his memory. I acknowledge also the contributions of Dr. Mark Gould. Dr. Ganes Das, and Mr. Chris Lennard. I wish to thank Professor Francis Troyon, CRPP, Lausanne for his hospitality and for the facilities provided to use the ERATO code. This work has been supported by the Australian Research Grants Scheme.

REFERENCES

1. R. C. GRIMM, J. M. GREENE, AND J. L. JOHNSON, *Methods in Computational Physics*, edited by J. Killeen (Academic Press, New York, 1976), Vol. 16, p. 253.
2. D. BERGER, L. C. BERNARD, R. GRUBER, AND F. TROYON, *Nucl. Fusion* **18**, 1331 (1978); R. GRUBER, F. TROYON, D. BERGER, L. C. BERNARD, S. ROUSSET, S. SCHREIBER AND K. V. ROBERTS, *Comput. Phys. Comm.* **21**, 323 (1981).
3. W. KERNER, *Nucl. Fusion* **16**, 642 (1976).
4. G. BATEMAN, W. SCHNEIDER, AND W. GROSSMAN, *Nucl. Fusion* **14**, 669 (1974).

5. A. SYKES AND J. A. WESSON, *Nucl. Fusion* **14**, 645 (1974).
6. C.-M. RYU AND R. C. GRIMM, *J. Plasma Phys.* **32**, 207 (1984).
7. J. DIBIASE AND J. KILLEEN, *J. Comput. Phys.* **24**, 158 (1977).
8. J. DIBIASE, Ph. D. thesis, Univ. of California, Davis, UCRL-51591 1974 (unpublished).
9. J. P. FREIDBERG AND D. W. HEWETT, *J. Plasma Phys.* **26**, 177 (1981).
10. D. C. ROBINSON, J. A. DIBIASE, A. S. FURZER, J. KILLEEN, J. E. NUNN-PRICE, Culham Report, CLM-P710, 1983 (unpublished).
11. R. J. HOSKING, Australian *J. Phys.* **31**, 347 (1978).
12. H. P. FURTH, *Propagation and Instabilities in plasmas*, edited by W. T. Futterman (Stanford Univ. Press, Stanford, CA, 1963), p. 87.
13. D. D. SCHNACK AND J. KILLEEN, *J. Comput. Phys.* **35**, 110 (1980); D. D. SCHNACK, D. C. BAXTER, AND E. J. CARAMANA, *J. Comput. Phys.* **55**, 485 (1984).
14. B. V. WADDEL, M. N. ROSENBLUTH, D. A. MONTICELLO, AND R. B. WHITE, *Nucl. Fusion* **16**, 528 (1976).
15. B. CARRERAS, B. V. WADDELL, AND H. R. HICKS, *Nucl. Fusion* **19**, 1423 (1979).
16. A. I. SHESTAKOV, J. KILLEEN, AND D. D. SCHNACK, *J. Comput. Phys.* **46**, 69 (1982).
17. A. SYKES AND J. WESSON, *Phys. Rev. Lett.* **37**, 140, (1976).
18. R. G. STORER, R. C. GRIMM, AND M. D. GOULD, "Proc. Annual Controlled Fusion Theory," Sherwood Conf., Austin, TX, 1981, 1C29; R. G. STORER, "Proc. Int. Conf. on Plasma Physics," Göteborg, 1982, p. 66.
19. L. A. CHARLTON, B. A. CARRERAS, J. A. HOLMES, H. R. HICKS, AND V. E. LYNCH, "Proc. U.S.–Japan Workshop," Oak Ridge, TN, 1983.
20. H. P. FURTH, J. KILLEEN, AND M. N. ROSENBLUTH, *Phys. Fluids* **6**, 459 (1963).
21. H. P. FURTH, P. H. RUTHERFORD AND H. SELBERG, *Phys. Fluids* **16**, 7 (1973).
22. A. H. GLASSER, J. M. GREENE, AND J. L. JOHNSON, *Phys. Fluids* **18**, 875 (1975).
23. A. H. GLASSER, S. C. JARDIN, AND G. TESAURO, *Phys. Fluids*, **27**, 1225 (1984).
24. R. C. GRIMM, R. L. DEWAR, J. MANICKAM, S. C. JARDIN, A. H. GLASSER, AND M. S. CHANCE, "Proc. 9th Int. Conference in Plasma Physics and Controlled Nuclear Fusion Research" IAEA-CN-41, 1982; J. MANICKAM, R. C. GRIMM, AND R. L. DEWAR, "Proc. of the 10th IMACS World Congress on System Simulation and Scientific Computation," Montreal, 4, 1982, 175.
25. V. D. SHAFRANOV, *Zh. Tekh. Fiz.* **40** (1970); *Sov. Phys. Tech. Phys.* **15**, 175 (1970).
26. G. BATEMAN, *M.H.D. Instabilities* (MIT Press, Cambridge, MA, 1978).
27. G. BATEMAN AND R. G. STORER, *J. Comput. Phys.* in press.
28. D. POTTER, *Computational Physics* (John Wiley, London, 1973).
29. J. H. WILKINSON, *The Algebraic Eigenvalue Problem* (Oxford Univ. Press (Clarendon), London 1964).
30. R. G. STORER, *Plasma Phys.* **25** 1279 (1983).
31. L. S. SOLOV'EV, *Sov. Phys. JETP* **26**, 400 (1968).
32. D. BERGER, L. C. BERNARD, R. GRUBER, AND F. TROYON, *J. Appl. Math. Phys.* (*ZAMP*) **31**, 113 (1980).
33. W. KERNER, *Nucl. Fusion* **16**, 64 (1976).
34. M. S. CHANCE, J. M. GREENE, R. C. GRIMM, J. L. JOHNSON, J. MANIKHAM, W. KERNER, D. BERGER, L. C. BERNARD, R. GRUBER, AND F. TROYON, *J. Comput. Phys.* **28**, 1 (1978).
35. G. BATEMAN AND Y.-K.M. PENG, *Phys. Rev. Lett.* **38**, 829 (1977).
36. J. L. JOHNSON, H. E. DALHED, J. M. GREENE, R. C. GRIMM, Y. Y. HSIEH, S. C. JARDON, J. MANICKHAM, M. OKABAYASHI, R. G. STORER, A. M. M. TODD, D. E. VOSS, AND K. E. WEIMER, *J. Comput. Phys.* **32**, 212 (1979).
37. F. TROYON, R. GRUBER AND H. SAURENMANN, S. SEMANZATO, AND S. SUCCI, *Plasma Phys. and Controlled Fusion* **26**, 209 (1984).